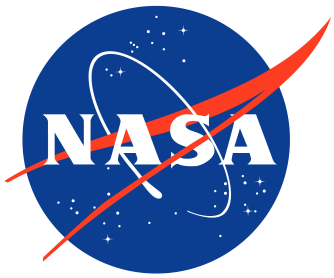

Assembly of the FOXSI-4 Mirror Modules

National Aeronautics and Space Administration

Assembly of the FOXSI-4 Mirror Modules

Stephen D. Bongiorno[a], Wayne H. Baumgartner[a], Jeffery Kolodziejczak[a], Charles G. Davis[b], Jagan Ranganathan[a], Nicholas Thomas[a], Jeff McCracken[c], and Danielle Gurgew[d]

[a]NASA MSFC, Huntsville, AL, USA
[b]Polaris Sensor Technologies, Huntsville, AL, USA
[c]Manufacturing Technical Solutions, Huntsville, AL, USA
[d]Universities Space Research Association, Huntsville, AL, USA

ABSTRACT

The Focusing Optics X-ray Solar Imager 4 (FOXSI-4) is a heliophysics sounding rocket experiment that is currently in its fourth launch campaign. The payload is comprised of seven x-ray telescopes, which each consist of a 2 m focal length grazing incidence mirror module that focuses x-rays onto an imaging detector. For this fourth flight, Marshall Space Flight Center (MSFC) designed, built, and tested three new high-angular-resolution mirror module assemblies (MMAs). This paper describes the design and assembly of the FOXSI-4 MMAs.

Keywords: FOXSI-4, x-ray, optics, full-shell optics, grazing incidence

1. INTRODUCTION

The Focusing Optics X-ray Solar Imager (FOXSI) is a NASA sounding rocket experiment, the primary goal of which is to study the sun in x-rays using focusing optics. Two prominent questions that the FOXSI experiment aims to investigate are how the Sun is able to efficiently transfer magnetic to kinetic energy in solar flares and how the solar corona maintains a temperature of $\sim$2 million degrees despite the underlying photosphere being a much cooler 5800K. In addition to advancing understanding of extreme solar events, answering these questions may yield insight into the fundamental physics of astrophysical plasmas. In solar flares, electrons in the solar atmosphere are accelerated by changing magnetic fields and subsequently emit Bremsstrahlung x-rays. Bremsstrahlung intensity is proportional to ambient plasma density, making flare-related x-ray emission brightest at the footprint of flare loops and significantly less intense in regions of the flare that reach higher up in the solar atmosphere, presumably in the corona. Making observations to study this science case requires an instrument with both high angular resolution, to resolve and distinguish between distinct emission regions, and high sensitivity, to detect low surface brightness x-ray emission higher up in the solar atmosphere. The focusing x-ray optics designed for FOXSI meet both of these requirements.

Thus far, FOXSI has had three successful launches.[1–3] The first three launch campaigns made FOXSI the first solar-dedicated instrument to observe the sun with focusing optics in hard x-rays. Planned for March 2024, the fourth FOXSI flight will be part of a solar flare campaign, where the FOXSI-4, Hi-C FLARE, and SNIFS sub-orbital payloads will launch near-simultaneously and observe a solar flare concurrently with the Parker Solar Probe. In all previous launches, FOXSI flew from the White Sands Missile Range. However, the fourth campaign will fly from Poker Flat Alaska because this site offers the flexible launch schedule required to wait for a solar flare.

For FOXSI 1-3, NASA Marshall Space Flight Center (MSFC) built all of the focusing optics that gather light in the FOXSI telescopes. For FOXSI-4, MSFC designed, built, vibration tested, and x-ray calibrated three new high-angular-resolution optical modules. This proceedings paper will describe the assembly process of the FOXSI-4 mirror modules from a post-build perspective. The module design will be described in §2, shell alignment process development will be described in §3, the flight assembly will be described in §4, and finally, §5 summarizes the reported results.

Further author information: (Send correspondence to S.D.B.)
E-mail: stephen.d.bongiorno@nasa.gov

2. MIRROR MODULE DESIGN

The FOXSI payload, shown in Figure 1a, consists of seven co-aligned telescopes, each comprised of a grazing incidence, full-shell mirror module assembly (MMA) and a pixelated detector located at the 2 m focal length of the optics. Each module contains multiple co-aligned electroformed nickel replicated shell optics. This payload design takes advantage of the replicated nature of electroformed optics in that one set of mandrels, which are relatively time-consuming to fabricate, may be used to replicate many shells and produce multiple modules to build up effective area at relatively low cost. In addition, the multiple telescope design allows for the simultaneous flight of new and heritage optics and detectors and both soft and hard x-ray detectors. For FOXSI-1 and -2, MSFC fabricated 10 unique mandrels. Those same mandrels have been used to replicate shells for FOXSI-3 and -4.

For FOXSI-4, MSFC improved the electroformed nickel shell replication process that has nearly three decades of heritage at the Center.[1–7] In this process, a thick aluminum mandrel is rough machined to the shape of the optical prescription, coated with electroless nickel, diamond turned, polished, passivated, and submerged in an electroforming bath where a nickel cobalt shell is grown on top of the mandrel. The shell-mandrel is then submerged in a cold water bath where the shell releases, producing a high-fidelity replication of the polished mandrel surface figure and roughness on the inside of the shell. After release, the shell interior surface is sputter coated with 100 Å of iridium to increase hard x-ray reflectivity.

The FOXSI optics are monolithic Wolter 1 full-shells, meaning that the parabolic (P) and hyperbolic (H) optical surfaces are formed in one piece of shell material. This design is advantageous because it does not require P-H segment alignment, is inherently stiffer than separate P and H segments, and has approximately half the edge-affected region of a design with separate P-H segments. Details on the FOXSI mirrors are shown in Table 1. As is standard practice with x-ray mirror modules, the 10 FOXSI Wolter 1 optical prescriptions are defined such that the replicated shells can be nested inside one another. This is a volume-efficient strategy for meeting a mirror module effective effective area requirement. As shown in Table 2, MSFC has built FOXSI optics in a variety of configurations.

Table 1: The FOXSI mirror module assemblies

Parameter	Value
Number of mirror modules on flight	7
Number of shells per mirror module	2 - 10
Prescription	Wolter 1
Focal length	2.0 m
Total shell length	607.8 mm
Range of shell intersection diameter	63.40 - 103.02 mm
Shell material	Nickel-cobalt alloy
Reflective coating	100 Å iridium

Table 2: New optics built by MSFC for each of the FOXSI launch campaigns.[3]

Launch Campaign	FOXSI	FOXSI-2	FOXSI-3	FOXSI-4
Launch date	11/2/2012	12/11/2014	9/7/2018	Planned 3/2024
Angular resolution (arcsec FWHM)	~ 5	~ 5	6.6, 7.5	~ 2.5
Number of shells per module	7 7-shell	2 10-shell	2 10-shell	3 2-shell
Shell thickness (μm)	300	300	300	520

The FOXSI-4 MSFC mirror module, shown in Figure 1b, consists of two optical shells, a front spider to which the shells are mounted, a housing structure that attaches to the front spider, and a mounting flange and rear spider that attach to the housing.

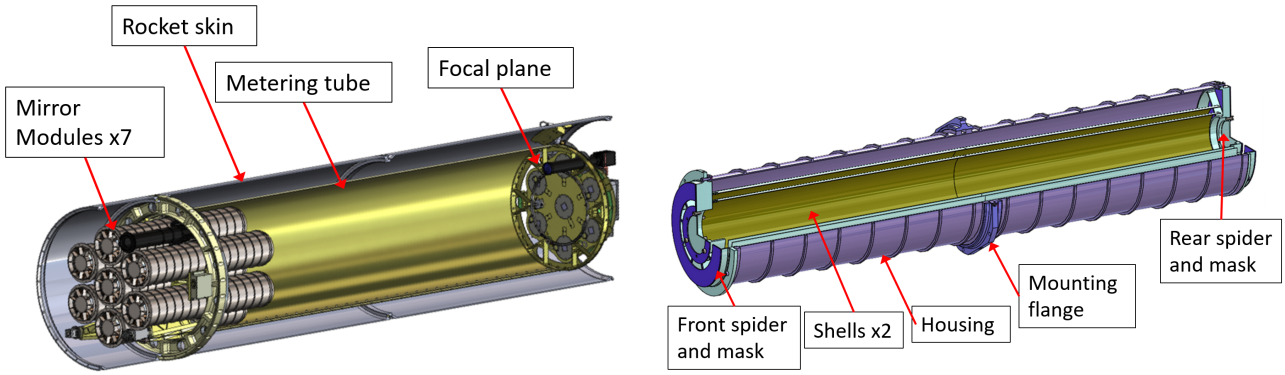

(a) FOXSI payload (b) MSFC FOXSI-4 MMA

Figure 1: Mechanical models

3. FOXSI-4 DEVELOPMENT

The primary goal of FOXSI-4 development at MSFC was to produce mirror modules with higher angular resolution. Toward that goal, development focused on three main areas: mandrel polishing, shell replication, and shell alignment.

To improve the optical figure of the mandrel, two of the FOXSI mandrels were chosen to be repolished with the Zeeko IRP600X CNC polishing machine at MSFC. The deterministic polishing process consists of iteratively measuring the mandrel axial figure error on an interferometer and selectively polishing regions with larger height error. The use of progressively smaller CNC polishing tools enables efficient improvement of the optical figure across a range of spatial scales. All available polishing resources were devoted to repolishing the first and third FOXSI mandrels, which are named M19 and M15, respectively. A combination of deterministic polishing on the Zeeko machine and conventional lap superpolishing was used to maintain < 4 Å RMS surface roughness and achieve a best figure result of 0.9 arcsec HPD predicted performance in the spatial frequency band affected by the 10 mm polishing bonnet, on the H-side of the M15 mandrel. Skipping the second mandrel and only polishing and mounting shells from the first and third mandrels was done for two reasons: so that the shells could be made thicker without vignetting one another and so that the two shells did not contact during launch vibration. The shell thickness was increased from the 300 μm used on FOXSI 1-3 to 520 μm on FOXSI-4 to reduce shell distortion during separation from the mandrel. A given separation shear stress at the shell-mandrel interface, which is characteristic of the passivation and separation process, is expected to cause less yielding of a thicker, stronger shell. Details on the mandrel polishing process will be presented in a proceedings paper by Baumgartner et al.[8]

To better understand and improve the shell replication process, the electroforming bath was modeled and optimized with COMSOL multiphysics software. In the bath, electric field strength is proportional to deposition current, which is correlated to as-deposited stress of the shell material. The primary goal of the optimization was to minimize electric field non-uniformity because this is expected to reduce stress gradients and therefore reduce shell distortion. Details on FOXSI-4 electroforming bath modeling will be presented in a proceedings paper by Singam et al.[9]

Finally, the shell alignment and bonding process was improved. The remainder of this paper will describe these design improvements and the flight shell alignment results.

3.1 EPOXY SHRINKAGE

A common technique for minimizing distortion when mounting fill-shell x-ray optics is to glue the shells to a spider structure with radial spokes. On FOXSI, the spider was built to typical machining tolerances (± 10 μm) while the shell optic must be maintained to optical tolerances (~ 0.2 μm). In order to attach the two together while minimally distorting the shell, liquid adhesive is applied in the gap between the two, accommodating the tolerance mismatch. Unfortunately, nearly all epoxies shrink during cure due to a change in density during the

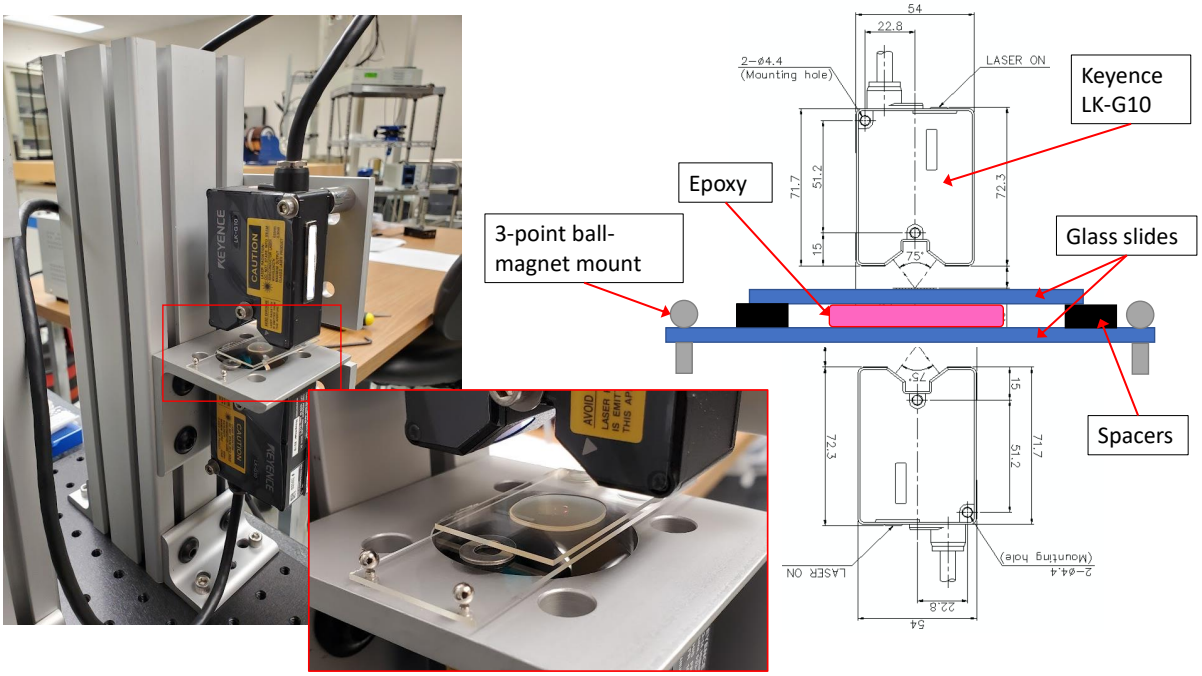

Figure 2: An annotated drawing of the epoxy shrinkage measurement apparatus.

phase change from liquid to solid. This shrinkage can distort optics when they are bonded to the mirror module assembly.

In the optical modules built for previous FOXSI launch campaigns, Loctite EA9313 adhesive was used to bond the mirror shells to an intermediate "clip" structure and Optocast 3553 UV-cure adhesive was used to bond the clip to the front spider. With its short cure time, Optocast 3553 was originally chosen so that multiple shells could be aligned and bonded to a module in one day. For FOXSI-4 development, minimizing optical distortion, and therefore minimizing epoxy shrinkage, was prioritized over minimizing the module assembly duration. To compare shrinkage between the two epoxies, an apparatus, shown in Figure 2 was built.

In the apparatus, a microscope slide is placed on a 3-point magnet mount where it is secured with three ball magnets. Three spacers are measured in thickness and placed on the slide. A volume of glue is dispensed onto the slide and covered with a glass coverslip. Displacement sensors are then positioned above and below the slides such that they measure the change in distance of the top surface of the cover slip and bottom surface of the glass slide as the epoxy cures. The displacement sensors have a spot size of approximately 20 μm that is positioned at the center of the epoxy droplet. Knowing the spacer thickness and displacement sensor data, the linear shrinkage of the epoxy can be measured during cure.

Independent shrinkage measurements were made with both of the test epoxies. EA9313 was mixed according to the manufacturer's technical datasheet in 4:1, resin to hardener ratio. Temperature in the lab was monitored with a calibrated Omega OM-CP-PRHTEMP2000 sensor that was mounted next to the shrinkage measurement apparatus. Optocast 3553 was cured for 3 minutes with an EFOS Novacure 2100 UV source. UV flux exiting the source light guide was measured at 2000 mW cm^{-2} using the device's built-in radiometer. Using the radiometer, transmission of the coverglass was measured to be approximately 33%. During cure, the expanding beam of the 0.25 inch diameter light guide beam was positioned such that it filled the 0.5 inch diameter epoxy droplet, reducing flux by a factor of 4. Therefore, during cure, the droplet was receiving a UV flux of approximately 160 mW cm^{-2} and during the 3 minute cure, received a total dose of 38 joules. The epoxy layer thickness was defined by the spacers, which were measured to be 0.79 mm thick.

For both epoxies, strain data were acquired until the expected cure time elapsed and a stable condition was

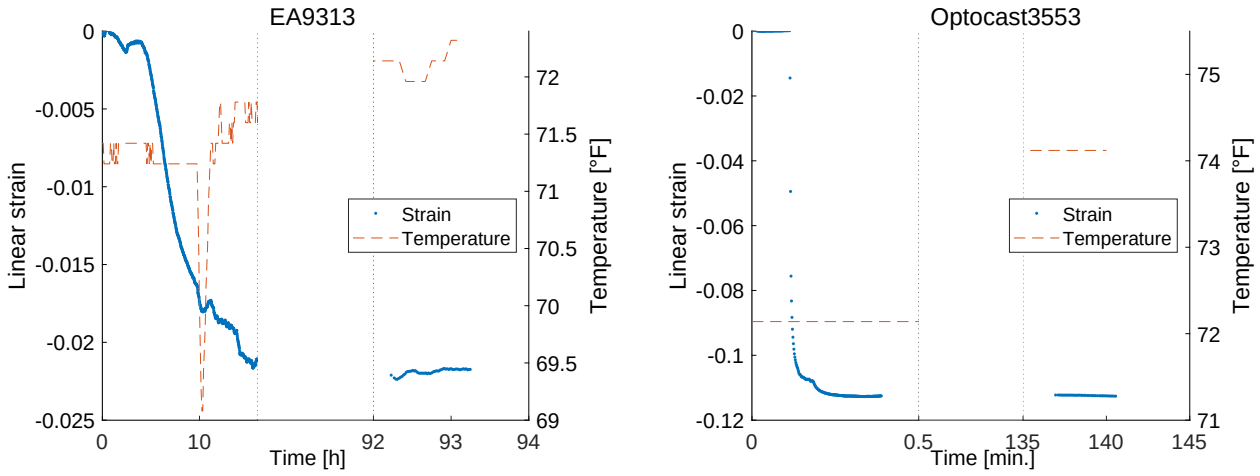

(a) Loctite EA9313 (b) Optocast3553

Figure 3: Simultaneous cure-related strain and temperature data for two FOXSI heritage epoxies. Data are shown in one interval at the start of cure and a second interval after the expected cure time elapsed. Strain has been zeroed to the value at the beginning of cure.

reached. Data are shown in Figures 3a and 3b. The linear shrinkage measured in EA9313 was 2.2% after 93 hours and 11.3% after 2.3 hours. The factor of 5.1 lower shrinkage exhibited by EA9313 prompted the project to switch from Optocast 3553 to EA9313 for bonding mirror shells.

One point of discussion on the epoxy shrinkage data is that of shrinkage uniformity across the sample. Micrometer thickness measurements of the cured samples showed that the coverglass became curved concave during the cure, indicating that the largest shrinkage occurred at the center of the sample. This is where the strain measurement was made, which makes the reported shrinkage values upper limits. Since both epoxies were tested in nominally identical configurations, this effect is not expected to affect the ratio between the two shrinkage measurements and therefore not expected to change the conclusion that EA9313 has lower shrinkage than Optocast 3553.

A second point of discussion on the epoxy shrinkage data is that of the mechanical stiffness of the coverglass and its effect on the shrinkage measurement. As seen in Figure 5, the coverglass slide that encapsulates the epoxy sample is suspended between spacers. The coverglass bends as the glue cures and its stiffness blocks shrinkage of the epoxy. To test whether this effect significantly reduces shrinkage measurements made with this apparatus, measurements of EA9313 were repeated with a 1 mm thick glass slide in place of the 0.15 mm coverglass. A shrinkage of 2.0% was measured. The bending stiffness of the glass slide was approximately 300 times larger than the coverglass and the shrinkage measured with the glass slide was a marginal 10% lower, indicating that the stiffness of the coverglass does not significantly influence the shrinkage measurement.

3.2 ALIGNMENT STATION IMPROVEMENTS

The FOXSI-4 shell alignment station is a laboratory apparatus that aligns, offloads, and stabilizes the mirror shells so that they can be bonded to the front spider with sufficiently precise optical node position, optical axis orientation, and figure. For the FOXSI, FOXSI-2, and FOXSI-3 MMAs, the shells were aligned with an apparatus that supported them at three points on the bottom (P) edge, leaving them distorted by self-gravity. For FOXSI-4, the decision was made to reduce self-gravity distortion by switching to the wire suspension alignment station design built for the *IXPE* program.[10] Shown in Figure 4, an *IXPE* alignment station was substantially upgraded for FOXSI-4. The original design consisted of a central kinematic mount for aligning the MMA front spider, an upper rig with hanging support wires for hanging an offloaded shell in position over the front spider assembly, and a spin table for rotating the sensor tower around the shell to measure its position and shape. To reduce distortion due to self-gravity, the alignment station suspends the shell over the front spider assembly from the top edge via three direct support suspension wires and three offload wires. The direct support wires are actuated

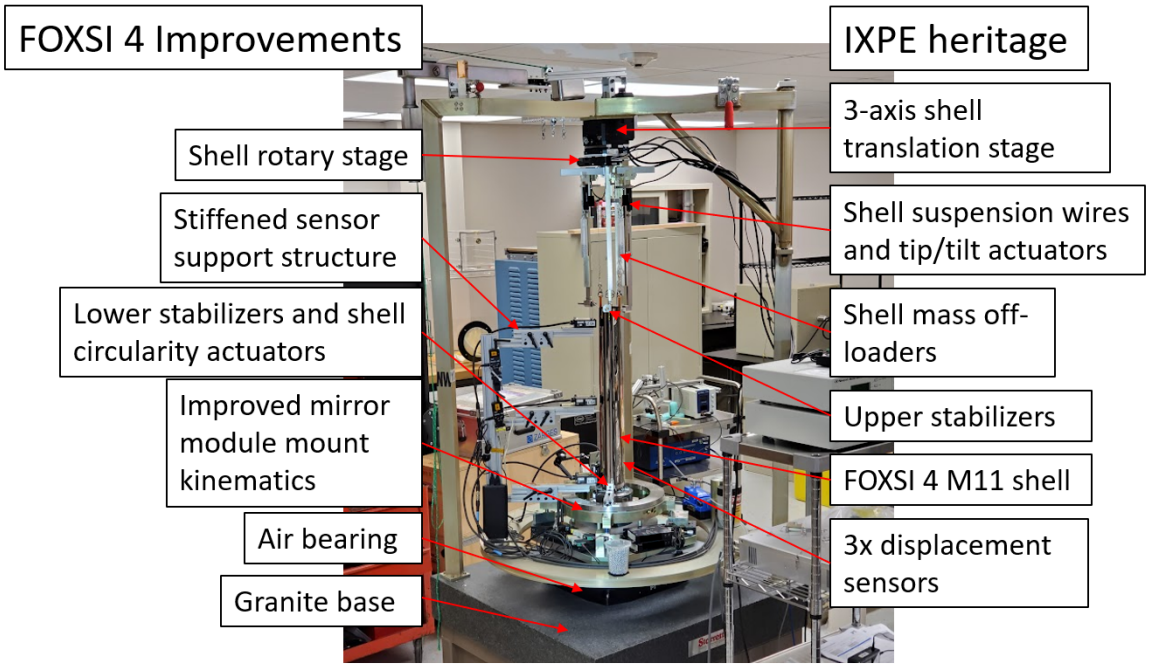

Figure 4: An annotated picture of the FOXSI-4 alignment station. Labels on the left point to design improvements made for FOXSI-4, while labels on the right point to heritage IXPE design features. The FOXSI M11 shell in this image was not used for flight.

in the vertical direction, enabling adjustment of shell tip and tilt. The three adjustable offloaders pull upwards on the shell with $1/6^{\text{th}}$ of its weight to reduce trefoil distortion induced by the three direct support points.

For FOXSI-4, the displacement sensor tower was stiffened to reduce vibration-induced noise and improve alignment of the sensors, the spin table was upgraded to an air bearing to reduce wobble of the sensor motion, a rotary stage was added to the top rig to enable clocking rotation of the shell, lower stabilizer actuators were added to stabilize and adjust circularity of the shell, and the entire apparatus was mounted to a granite table.

3.3 SHELL ALIGNMENT METHODOLOGY

Before bonding the shells to the front spider, the shell optical nodes must be centered and optical axes aligned with respect to one another. Misalignment of the shell optical axes weakly degrades effective area and angular resolution and may cause mechanical interference between shells. Misalignment of the shell optical nodes degrades the PSF as $\text{HPD}_{\text{decenter}} \approx \delta/f$, where δ is the magnitude of decenter between the optical node of two optics and f is the focal length. The alignment station must also hold the shells in a minimally stressed state, such that their own self-weight does not cause significant shape distortion. Distortion of a shell due to holding will be permanently imprinted in the optic once it is bonded in place.

The shell alignment measurements were made with displacement sensors positioned near the small end, intersection, and large end of the shell. The sensors rotate around the shell via the alignment station spin table and were sampled at approximately 500 azimuths. This produces displacement waveforms that represents the shell's relative deviation from a circular shape (minus spin table bearing error). Note that while the absolute radius of the shell cannot be determined with this measurement, it is not needed for calculating the relevant shell alignment parameters. The rotation axis of the spin table bearing is the reference for all alignment station measurements performed during the shell installation process. In these displacement waveform data, shell centering error appears as an approximately sinusoidal waveform that peaks once per revolution, shell ovality peaks twice per revolution, shell trefoil peaks three times, etc. Fitting a line in three dimensions to the shell centering error in the top, middle, and bottom sensors enables calculation of the shell tilt. Data from two sensors are sufficient to calculate the shell optical axis angle and node position with respect to the station

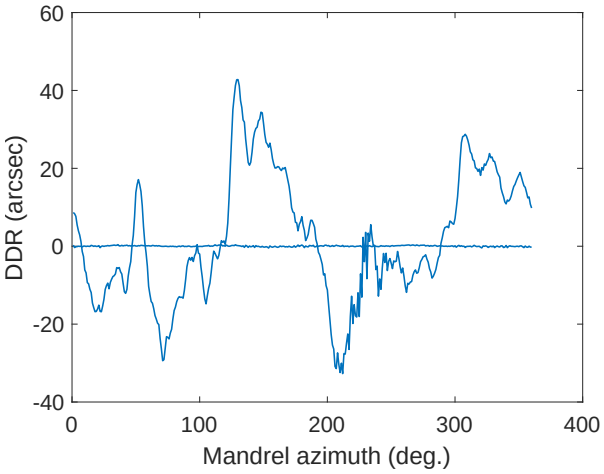

(a) The ART-XC M25 mandrel measured on *IXPE* alignment station 3, exhibiting 45.5 arcsec HPD DDR. For reference, the data in Figure 5b, has been overplotted.

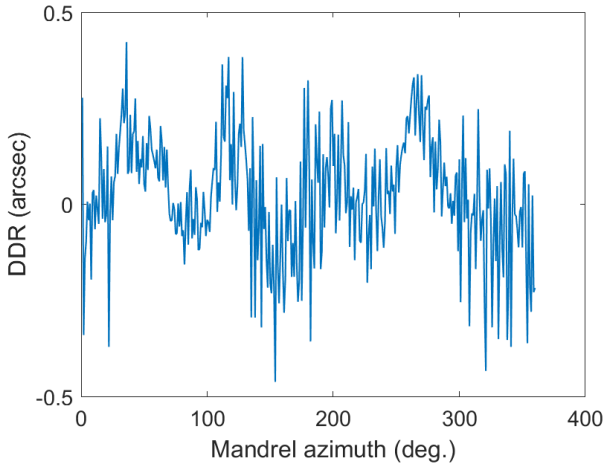

(b) The ART-XC M18 mandrel measured on the enhanced FOXSI alignment station, exhibiting 0.4 arcsec HPD DDR.

Figure 5: Alignment station mandrel measurement results.

rotation axis. Data from a third sensor was used to calculate deviations in bending of the shell along each azimuth. Knowing the axial distance between sensors, the difference between the top and center, and bottom and center sensor readings can be used to calculate the change in angle of the top and bottom segments of the shell. Adding these two angles yields the change in intersection angle of the shell as function of azimuthal angle, ϕ. We call this quantity delta delta radius, DDR(ϕ), and it is an indicator of low spatial frequency shape error. If errors are Gaussian-distributed, the DDR-predicted half-power diameter, $\mathrm{HPD}_{\mathrm{DDR}}$, of the optic point spread function (PSF) will be $\mathrm{HPD}_{\mathrm{DDR}} = 2.698$ RMS(DDR(ϕ)). However, in the case of a FOXSI shell, structure of the DDR waveform is dominated by low order cyclic harmonic functions (oval, trefoil, etc.) and the equivalent HPD is $\mathrm{HPD}_{\mathrm{DDR}} = 4$ RMS(DDR(ϕ)). With no assumed model, HPD can be calculated as $\mathrm{HPD}_{\mathrm{DDR}} = 4$ median(abs(DDR(ϕ))).

A MATLAB application based on the software used for *IXPE* shell alignment was modified for FOXSI-4 MMA assembly and used to partially automate the iterative aspects of the shell alignment process. First, the application reads and analyzes sensor data and calculates shell center, tilt, and a DDR performance estimate. The application automatically adjusts the shell position in 5 axes (3-axis translation stage and 2 of 3 actuators supporting direct support wires) to align the shell. Finally, the application allows for manual adjustment of stages, direct support actuators, and circularity adjustment actuators. Typically, ten iterations were required to align a shell, depending on initial state, to reach $\sim$1 arcsecond tilt and $\sim$1 μm centering.

3.4 ALIGNMENT STATION COMMISSIONING

To characterize the performance of the shell alignment station, a flight mandrel was mounted in place of a shell. The mandrels are thick aluminum parts that have been diamond turned; they are expected to be extremely circular and suitable as a reference for the alignment station. Figures 5a and 5b show the dramatic performance increase by upgrading the sensor rotation stage bearing. With post-processing to subtract the bearing error, the *IXPE* alignment station results were estimated to have an error of $\pm$5 arcsec. With similar post-processing and additional sensor calibration, we expect the FOXSI alignment station metrology to be suitable for measuring sub-arcsecond optics.

3.5 ALIGNMENT STATION THERMAL SENSITIVITY

During shell assembly it was observed that the position of a suspended shell was correlated with the ambient air temperature. To characterize this effect, shell FOXSI4-M19S10 was measured with the alignment station as the room temperature changed. Figure 6 shows correlations between the shell optical node position, shell optical

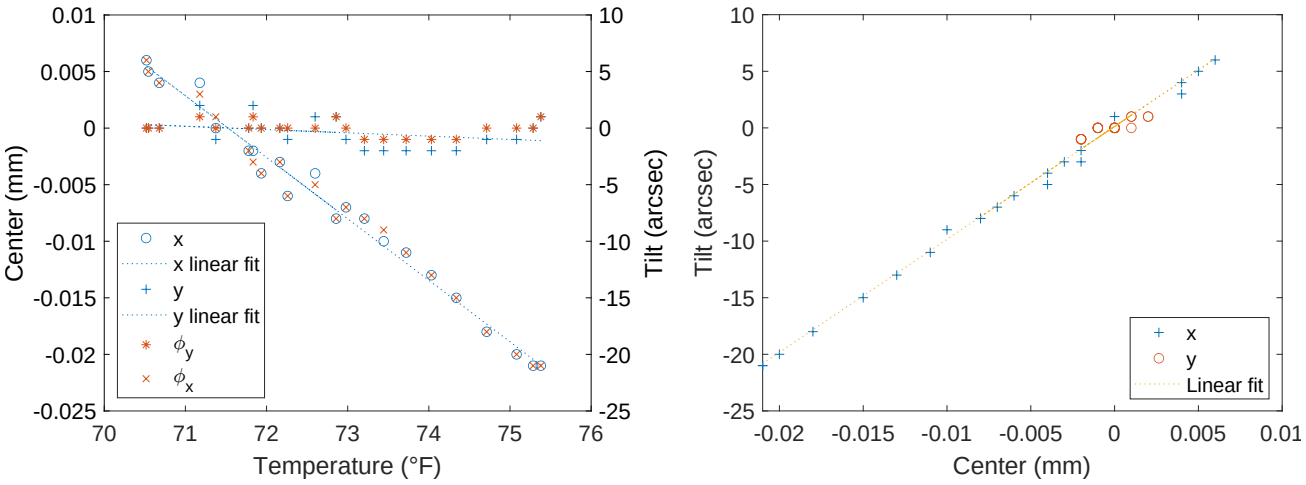

(a) Shell alignment parameters as a function of ambient temperature.

(b) Shell optical axis tilt as a function of shell optical node position.

Figure 6: Temperature stability of a single shell on the alignment station.

axis angle, and the room temperature. Figure 6a shows the optical node position (blue markers) in the x and y axes as a function of temperature. There is a strong correlation between node position and temperature in the x direction, with the slope of a linear fit to the x optical node position being -5.4 μm $^{\circ}\mathrm{F}^{-1}$. In the y direction, the slope is -0.3 μm $^{\circ}\mathrm{F}^{-1}$. Figure 6b shows the correlation between the optical node position and the tilt, with the slope and y-intercept of the linear fit being 997 arcsec mm^{-1} and 0.13 arcsec, respectively. This corresponds to rigid body motion of the shell rotating about a point on the optical axis located 207 mm from the optical node, toward the shell entrance aperture. This metrology-derived center of rotation is close to the position of the shell lower support points, which were positioned 275 mm from the optical node. This indicates that the temperature-induced drift of the shell is almost entirely due to movement of the upper shell alignment station structure.

3.6 ALIGNMENT STATION SETUP SENSITIVITY

To gain confidence in the alignment station before proceeding with flight assembly, we measured the sensitivity of FOXSI shell shape to errors in position of the support wires and offloader mass. In the first experiment, direct support wires were moved away from their nominal position and the shape of a FOXSI4-M15S12 shell measured with the alignment station. In a second experiment, with the direct supports in their nominal positions, an offloader mass was changed and the shape of FOXSI4-M15S12 was again measured with the alignment station. The results of both experiments are shown in Table 3. Given that the support wire location and offloader mass errors tested in this experiment were approximately 50 and 5 times higher, respectively, than expected errors and a significant shell performance decrement was not detected, we conclude that the shell alignment station process is currently insensitive to these errors.

Table 3: Alignment station setup sensitivity experiment results. 'NE −3.7 mm' denotes that the Northeast direct support was moved -3.7 mm from nominal, 'all −3.7' denotes that all direct supports were moved -3.7 mm, 'E +5g' indicates that 5 g was added to the East offloader, etc. Repeatability of the $\mathrm{HPD}_{\mathrm{DDR}}$ measurement is approximately ±0.1 arcsec.

Configuration	Baseline	NE −3.7 mm	all −3.7 mm	all +3.7 mm	E +5g	E +10g
$\mathrm{HPD}_{\mathrm{DDR}}$ (arcsec)	1.2	1.4	1.4	1.4	1.2	1.2

4. FLIGHT MIRROR MODULE ASSEMBLY

Beginning in April 11, 2023 and ending in June 1, 2023, three FOXSI-4 mirror modules were assembled serially on one alignment station at MSFC. The assembly environment was maintained at a temperature of $22.5 \pm 2°C$ and a relative humidity of 33-55% approximately 79% of the time. Bonding operations were paused when environmental properties were out of tolerance.

The MMA assembly process began with installing the front spider on the alignment station via a three-point, bolted attachment. Sets of lapped spherical washers were placed above and below the attachment bolts. This design minimizes bending moments on the spider, which is important because any bending preload placed on the spider at this early stage of assembly will be present when the shells are bonded in place. After shell assembly, unbolting the preloaded MMA from the alignment station will cause the spider to bend back to near original shape and permanently distort the shells. After the front spider was attached to the station, a displacement sensor was used to align the front spider to the station sensor rotation axis by adjusting the mirror module kinematic mount. The smallest shell was then transferred from a storage container to the alignment station using the station transfer arm, where it was inspected, attached to the station wire suspension, and the bond areas primed with an adhesion promoter. The shell tilt and position were measured with the alignment station and aligned with actuators on the direct support suspension wires and the 3-axis translation stage in the upper rig, respectively.

After a shell was hung on the alignment station, initial alignment was performed with the shell, free-hanging, above the front spider spokes. A small pendulum motion was observed from room air currents acting on the shell. Mechanical stabilizers were installed at the top (H) edge of the shell to stop the pendulum motion while minimizing any translation of the shell from the bottom of the gravitational potential well. The shell was then realigned, lowered to final position above the spider and realigned again. In this configuration, it was observed that while the shell did not exhibit free-hanging pendulum motion, the alignment was unstable. Lower stabilizer actuators were used to reduce this instability and allow tip/tilt and translation of the shell. When the shell was stabilized at the top, the upper 3-axis translation stage and shell suspension wire actuators were used to adjust position and tip/tilt, respectively. In this configuration, the alignment algorithm assumes that tip/tilt adjustments cause the shell to rotate about a point at the intersection between the optical axis and the top (H) edge of the shell. When the shell is stabilized at the top and bottom, the upper 3-axis translation stage and the lower stabilizer actuators are used together to adjust the translation and tip/tilt of the shell and the alignment algorithm is changed accordingly.

4.1 SHELL ALIGNMENT RESULTS

Shell alignment results of the FOXSI-4 optics are shown in Table 4. To improve co-alignment, the M15 (larger) shell was aligned to the center and tilt of the previous shell in all MMAs. For MMAs X9 and X11, the shells were bonded at approximately 8 PM because the subsequent 8 hour period was found to be the most thermally stable in the lab. For MMA X10, shell M15S12 was continuously realigned as the epoxy cured, which explains the substantially improved optical axis and optical node position co-alignment result. Table 5 shows the measured shell DDR before and after epoxy cure and the alignment station predicted module HPD. There was no measurable effect on shell performance due to epoxy cure. To calculate the alignment station predicted HPD, the contribution of each shell was weighted by the shell geometric effective area. Note that the alignment station is only probing the shell at three axial locations, so these performance predictions only account for the largest figure distortions in the shell.

Given the 0.6 arcsec HPD DDR alignment station bearing performance, 1 μm and 1 arcsec shell alignment capability of the alignment station, and sub-arcsec contribution of epoxy shrinkage to the optical figure, we expect this hardware and these processes to be capable of assembling an optic with performance of approximately 1 arcsec HPD.

*To achieve improved shell co-alignment in module X10, shell FOXSI4-M15S12 was continuously realigned as the epoxy cured.

Table 4: Shell alignment results for the FOXSI-4 mirror module assemblies. Columns x and y are the position of the optical node relative to the alignment rotation axis. $+y$ points in the direction of the MMA alignment mark and $+z$ points from the optical node to the exit aperture of the optics. $\sqrt{\delta x^2 + \delta y^2}$ is the magnitude of position change between the optical nodes of the two optics. $+\phi_x$ is a rotation of the optical axis from $+z$ toward $+x$ and $+\phi_y$ is a rotation from $+z$ toward $+y$.

MMA	Shell	x (μm)	y (μm)	$\sqrt{\delta x^2 + \delta y^2}$	ϕ_x (arcsec)	ϕ_y (arcsec)
X9	M19S06	-3	4	8	-3	-1
	M15S09	5	5		6	0
X10	M19S07	6	1	1*	9	2
	M15S12	5	1		8	1
X11	M19S08	3	2	4	3	2
	M15S13	5	5		4	4

Table 5: Shell DDR for the FOXSI-4 mirror module assemblies before and after bonding.

MMA	Shell	4*DDR pre-bond (arcsec)	4*DDR post-bond (arcsec)	Circ. predicted HPD (arcsec) w/o decenter	w/ decenter
X9	M19S06	0.8	0.5	1.0	1.4
	M15S09	1.6	1.6		
X10	M19S07	1.8	1.7	1.4	1.4
	M15S12	0.7	0.7		
X11	M19S08	1.8	1.7	1.7	1.8
	M15S13	1.7	1.2		

4.2 SHELL CIRCULARITY CORRECTION

In addition to stabilizing and aligning the P-end (lower end) of a shell when it was suspended on the shell alignment station, radially directed actuators were used to correct circularity error of the shells. The actuators were arranged such that they radially opposed one another, they were aligned with the shape error of the shell, and inward travel of the actuators reduced shape error in the shell. With 4 actuators arranged this way, the apparatus was capable of correcting first-order, oval-shaped error in shell figure while still being able to adjust position of the shell optical node and alignment of the shell optical axis. Fortuitously, the large spatial scale shape error in the shells was dominated by oval-shaped error and the predicted performance of two shells was substantially improved with actuator correction. Shell M19S06 was improved from 3.2 to 0.7 arcsec HPD and shell M19S07 was improved from 6.9 to 2.1 arcsec HPD circularity predicted performance.

Figure 7 shows the DDR error for all FOXSI-4 flight shells, with the two shells that were subjected to circularity correction shown bold and in color. As evidence by both the the waveforms in Figure 7 and the 2*DDR performance listed in Table 4, the circularity predicted performance of both corrected shells was successfully brought in family with that of the remaining flight optics. Development is currently under way to apply higher-order circularity correction to shells. This development is focused on validating the alignment station metrology at the sub-arcsecond level and developing algorithms for optimal higher-order correction.

The circularity adjustment figure improvements were made permanent when the shells were bonded to the spider. Since the corrective actuation was applied approximately 20 mm from the bonds, nearly all of the corrective influence remained imprinted on the shells after the actuators, stabilizers, and suspension wires were removed, after the epoxy had cured.

5. SUMMARY

Three grazing incidence x-ray mirror modules were assembled at MSFC for the upcoming FOXSI-4 sounding rocket flight. A development effort was undertaken to improve the imaging performance of these mirror modules

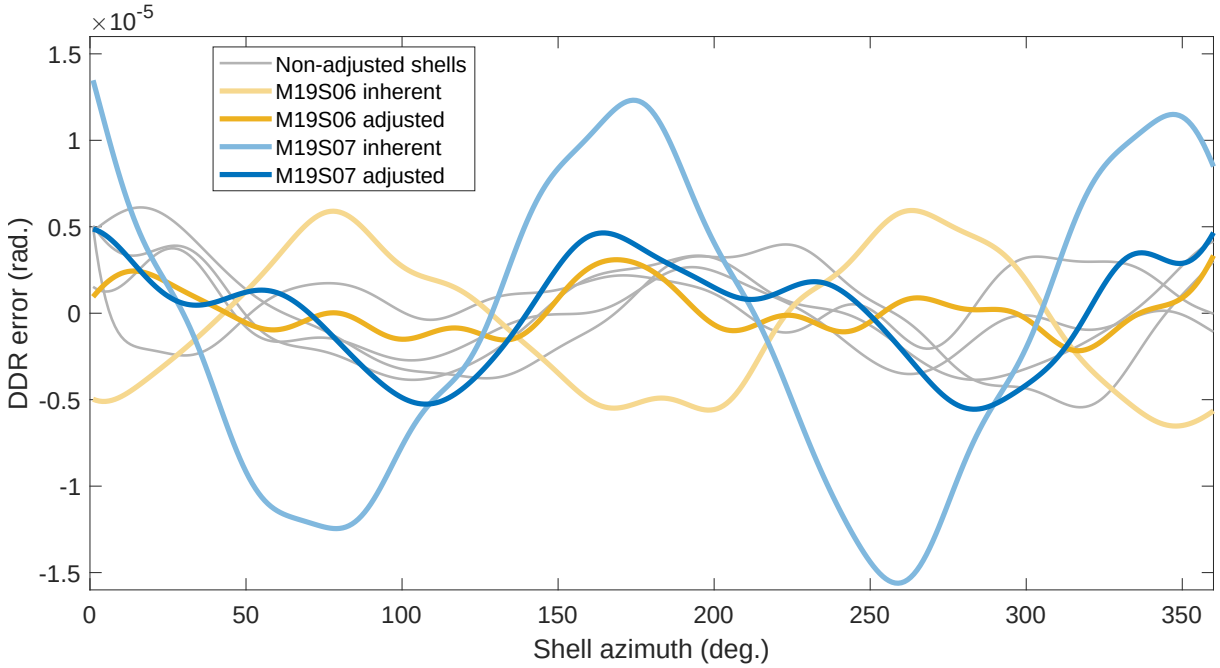

Figure 7: Shell circularity adjustment results. The light and dark blue and yellow lines show M19S07 and M19S06 DDR before and after circularity correction, respectively. The gray lines show the remaining 4 FOXSI-4 shells.

relative to those built for previous FOXSI campaigns. Related to alignment and mounting of the shell optics for FOXSI-4, an *IXPE*-heritage alignment station was improved and commissioned, and shell mounting procedures tested before assembling the FOXSI-4 flight optics. In two flight shells, the majority of oval-shaped figure error was corrected, placing their large spatial scale optical figure error in line with the remaining 4 flight shells. Shell co-alignment of approximately 1 μm and 1 arcsec was demonstrated and, ultimately, the alignment and mounting process was predicted to contribute < 1 arcsec HPD to the performance of the optics.

REFERENCES

[1] Krucker, S., Christe, S., Glesener, L., Ishikawa, S., Ramsey, B., Gubarev, M., Saito, S., Takahashi, T., Watanabe, S., Tajima, H., Tanaka, T., Turin, P., Glaser, D., Fermin, J., and Lin, R. P., "The focusing optics x-ray solar imager (FOXSI): instrument and first flight," in [*Solar Physics and Space Weather Instrumentation V*], Fineschi, S. and Fennelly, J., eds., **8862**, 88620R, International Society for Optics and Photonics, SPIE (2013).

[2] Christe, S., Glesener, L., Buitrago-Casas, C., Ishikawa, S.-N., Ramsey, B., Gubarev, M., Kilaru, K., Kolodziejczak, J. J., Watanabe, S., Takahashi, T., Tajima, H., Turin, P., Shourt, V., Foster, N., and Krucker, S., "FOXSI-2: Upgrades of the Focusing Optics X-ray Solar Imager for its Second Flight," *Journal of Astronomical Instrumentation* **5**, 1640005–625 (Mar. 2016).

[3] Glesener, L., Krucker, S., Christe, S., nosuke Ishikawa, S., Buitrago-Casas, J. C., Ramsey, B., Gubarev, M., Takahashi, T., Watanabe, S., Takeda, S., Courtade, S., Turin, P., McBride, S., Shourt, V., Hoberman, J., Foster, N., and Vievering, J., "The FOXSI solar sounding rocket campaigns," in [*Space Telescopes and Instrumentation 2016: Ultraviolet to Gamma Ray*], den Herder, J.-W. A., Takahashi, T., and Bautz, M., eds., **9905**, 99050E, International Society for Optics and Photonics, SPIE (2016).

[4] Ramsey, B. D., Engelhaupt, D. E., Speegle, C. O., O'Dell, S. L., Austin, R. A., Kolodziejczak, J. J., and Weisskopf, M. C., "HERO program: high-energy replicated optics for a hard-x-ray balloon payload," in [*EUV, X-Ray, and Gamma-Ray Instrumentation for Astronomy X*], Siegmund, O. H. W. and Flanagan, K. A., eds., **3765**, 816 – 821, International Society for Optics and Photonics, SPIE (1999).

[5] O'Dell, S. L., Jones, W. D., Ramsey, B. D., Engelhaupt, D. E., Smith, W. S., Cohen, L. M., and Speybroeck, L. P. V., "Development of Constellation-X optics technologies at MSFC," in [*X-Ray Optics, Instruments, and Missions III*], Truemper, J. E. and Aschenbach, B., eds., **4012**, 316 – 327, International Society for Optics and Photonics, SPIE (2000).

[6] Gubarev, M., Ramsey, B., O'Dell, S. L., Elsner, R., Kilaru, K., McCracken, J., Pavlinsky, M., Tkachenko, A., Lapshov, I., Atkins, C., and Zavlin, V., "Development of mirror modules for the ART-XC instrument aboard the Spectrum-Roentgen-Gamma mission," in [*Optics for EUV, X-Ray, and Gamma-Ray Astronomy VI*], O'Dell, S. L. and Pareschi, G., eds., **8861**, 88610K, International Society for Optics and Photonics, SPIE (2013).

[7] Ramsey, B. D., Bongiorno, S. D., Kolodziejczak, J. J., Kilaru, K., Alexander, C., Baumgartner, W. H., Elsner, R. F., McCracken, J., Mitsuishi, I., Pavelitz, S. D., Ranganathan, J., Sanchez, J., Speegle, C. O., Weddendorf, B., and O'Dell, S. L., "IXPE mirror module assemblies," in [*Optics for EUV, X-Ray, and Gamma-Ray Astronomy IX*], O'Dell, S. L. and Pareschi, G., eds., **11119**, 1111903, International Society for Optics and Photonics, SPIE (2020).

[8] Baumgartner, W. H., Bongiorno, S. D., Kolodziejczak, J. J., Singam, S., Gurgew, D. N., Speegle, C., Banks, D., Champey, P., Thomas, N. E., and Davis, C. G., "High resolution full shell replicated x-ray optics for FOXSI-4," International Society for Optics and Photonics, SPIE (2023).

[9] "," International Society for Optics and Photonics, SPIE (2023).

[10] Bongiorno, S. D., Kolodziejczak, J. J., Kilaru, K., Eng, R., Stahl, M., Baumgartner, W. H., Thomas, N., Ranganathan, J., Ramsey, B. D., and Tucker, J., "Assembly of the IXPE mirror modules," in [*Optics for EUV, X-Ray, and Gamma-Ray Astronomy X*], O'Dell, S. L., Gaskin, J. A., and Pareschi, G., eds., **11822**, 118220Y, International Society for Optics and Photonics, SPIE (2021).